Drug Discovery

To Cite:
Hossen Z, Islam MR, Hossain MS, Forhad MNU, Islam MR, Jubayer MA, Lisa AK, Hasan MF, Haque ME. Natural Compound-Based FLT3 Inhibition in Acute Myeloid Leukemia: A Comprehensive *In-Silico* Strategy Using Molecular Docking, ADME, and MD Simulation. *Drug Discovery* 2025; 19: e21dd3007
doi:

Author Affiliation:
[1]Department of Biotechnology and Genetic Engineering, Gopalganj Science and Technology University, Gopalganj 8100, Bangladesh
[2]Department of Biochemistry and Molecular Biology, Gopalganj Science and Technology University, Gopalganj 8100, Bangladesh
[3]Department of Microbiology, University of Rajshahi, Rajshahi-6205, Bangladesh

[*]**Corresponding Author**
Department of Biotechnology and Genetic Engineering, Faculty of Life Science, Gopalganj Science and Technology University, Gopalganj-8100, Bangladesh; Tel: +8801704-486239; Email: enamul.haque@gstu.edu.bd

Peer-Review History
Received: 29 April 2025
Reviewed & Revised: 15/May/2025 to 07/September/2025
Accepted: 18 September 2025
Published: 01 October 2025

Peer-Review Model
External peer-review was done through double-blind method.

Drug Discovery
pISSN 2278–540X; eISSN 2278–5396

Natural Compound-Based FLT3 Inhibition in Acute Myeloid Leukemia: A Comprehensive *In-Silico* Strategy Using Molecular Docking, ADME, and MD Simulation

Zubaer Hossen[1], Md Rezoanul Islam[2], Md Sajjad Hossain[1], Md. Naim Uddin Forhad[2], Md Raichul Islam[2], Abdullah-Al-Jubayer[1], Asura Khanam Lisa[1], Md. Faruk Hasan[3], Md. Enamul Haque[1]*

ABSTRACT

Acute myeloid leukemia (AML) with FLT3 mutations is a malignant blood cancer. However, current FLT3 inhibitors used in its treatment have significant side effects and drug resistance problems. Our study aimed to identify relatively safe and effective FLT3 inhibitors from natural phytocompounds to overcome the limitations of current therapies. A total of 2792 phytocompounds were collected from 19 medicinal plants and screened virtually against the FLT3 protein active site. Fifteen top compounds were selected based on docking scores. ADMET analysis and molecular dynamics (MD) simulation were performed to evaluate pharmacokinetics, toxicity, and stability. Three compounds — asperglaucide, 17beta-hydroxywithanolide K, and withanicandrin — showed strong binding affinities (−9.4, −10.1, and −10.9 kcal/mol, respectively), which were superior to the synthetic inhibitors gilteritinib (−9.1 kcal/mol). ADMET analysis confirmed favorable GI absorption, solubility, and low toxicity, comparable to gilteritinib. The 100-ns MD simulations (RMSD, RMSF, RG, SASA, hydrogen bonds) showed that asperglaucide formed the most stable protein-ligand complex. Natural compounds, especially asperglaucide, have shown promising potential as FLT3 inhibitors for the treatment of AML. Further in vitro and in vivo studies are needed to verify their therapeutic efficacy.

Keywords: Acute myeloid leukemia, FLT3 Inhibitors, Phytocompounds, Molecular Docking, ADMET Analysis, Molecular Dynamics Simulation

GRAPHICAL ABSTRACT

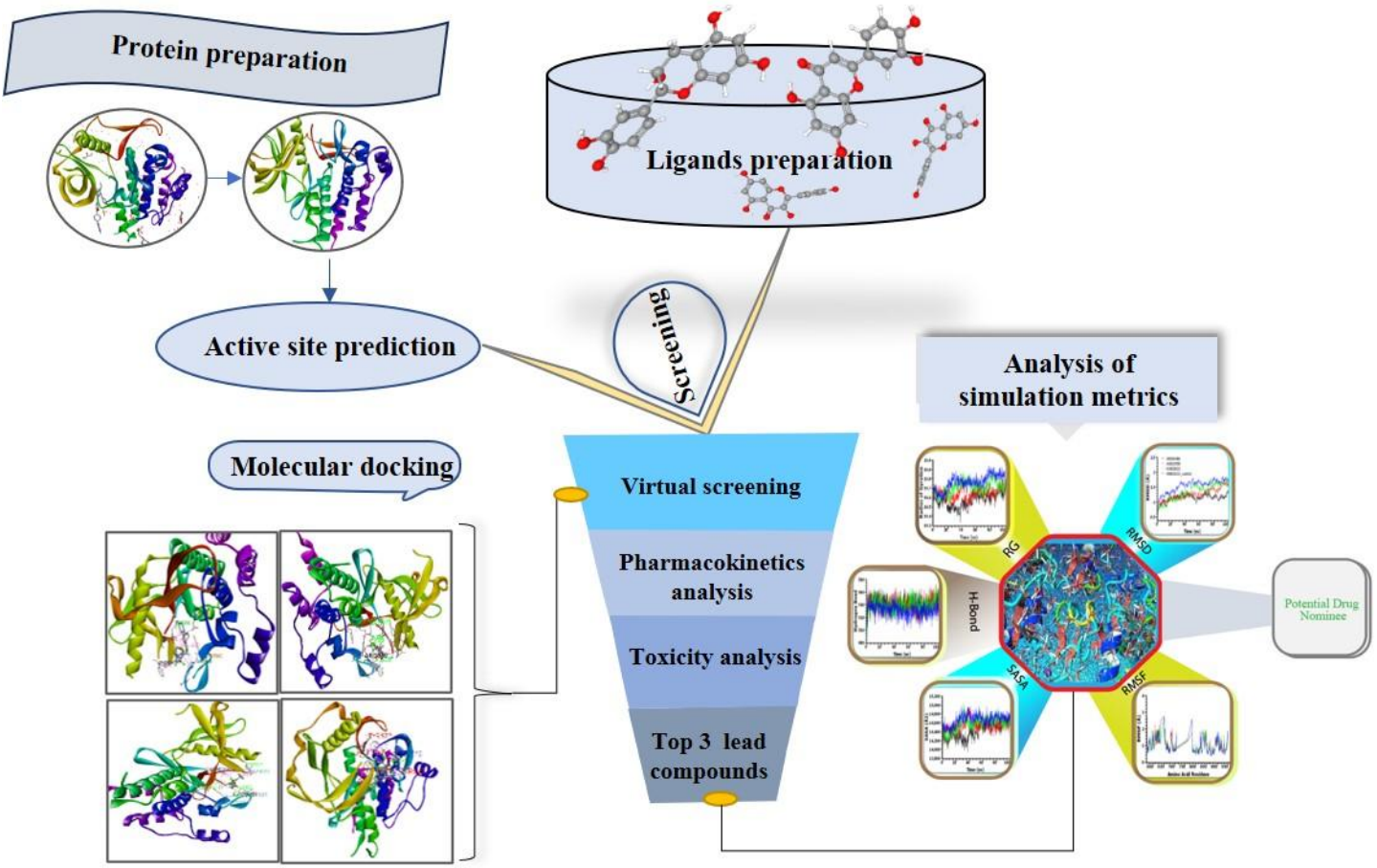

1. INTRODUCTION

Acute myeloid leukemia (AML) is a type of malignant blood cancer that disrupts the process of making normal blood cells in the bone marrow. The disease occurs when abnormal myeloid progenitor cells begin to grow and accumulate abnormally (PDQ Adult Treatment Editorial Board, 2002). These abnormal cells cannot differentiate into normal hematopoietic cells, which disrupts the normal process of producing red blood cells (RBCs), white blood cells (WBCs), and platelets in the blood (Döhner et al., 2015). Approximately 30% of AML patients have mutations or genetic changes in the FLT3 (Fms-like Tyrosine Kinase 3) gene. The most common and vital variant is FLT3-ITD (Internal Tandem Duplication). This results in abnormal activation of signaling pathways within the cell, such as PI3K/AKT, RAS/MAPK, and STAT5. The continuous activation of these signaling pathways leads to uncontrolled cell division, prolonged cell survival, and inhibition of programmed cell death or apoptosis. Collectively, these are responsible for the pathogenesis (development of the disease) and leukemogenesis (the process of leukemia formation) of AML (Döhner et al., 2015). For this reason, several FLT3 inhibitors targeting the FLT3-ITD and FLT3-TKD proteins have been developed, which are thought to be viable therapeutic targets in the treatment of AML (Stone et al., 2017; Perl et al., 2019). The efficacy of these inhibitors depends on their binding affinity to the FLT3 receptor (Kiyoi, Kawashima & Ishikawa, 2019). Structural studies have shown that FLT3 exists in two conformational variants—active and inactive. The difference between them depends on the specific arrangement of three amino acid residues (Asp-Phe-Gly) in the activation loop (Mirza et al., 2024). FLT3 inhibitors are divided into two groups depending on how they interact with these conformations, namely, type I and type II. Based on their binding preferences, type I inhibitors (such as midostaurin, gilteritinib, and crenolanib) can bind to both the active and inactive forms of FLT3 at the ATP-binding site, which increases their inhibitory potential (Abbas et al., 2019).

In contrast, type II inhibitors such as quizartinib and sorafenib selectively target the inner pocket of the ATP-binding region but only in the inactive conformation of FLT3, resulting in better selectivity (Kiyoi, Kawashima & Ishikawa, 2019; Daver et al., 2019). Despite their therapeutic relevance, both types of inhibitors have many side effects, some of which are potentially fatal, such as perimyocarditis (Kalkan et al., 2025), GI hemorrhage, respiratory failure, sepsis, and septic shock (Jiang et al., 2025), cardiac failure, pancreatitis, pneumonia, renal impairment, cytopenia, heart rhythm problems (QT prolongation), and stomach problems. In addition, drug resistance has been observed in many patients (Mecklenbrauck & Heuser, 2022). Therefore, we aimed to identify FLT3 inhibitors with fewer side effects and a better safety profile.

Compounds derived from many natural sources are considered necessary for their medicinal properties. Since ancient times, humans have used medicinal plants to treat various diseases. Unsurprisingly, many natural compounds show anticancer properties. Artemisia annua, a plant native to China and temperate regions of Asia, is used to treat malaria, fever, and digestive problems. Artemisinin, obtained from Artemisia annua, is of value in modern medicine (Septembre-Malaterre et al., 2020). Silymarin, obtained from Silybum marianum (Milk Thistle), a plant native to Mediterranean Europe, is used to treat liver diseases (Gillessen & Schmidt, 2020). Digitalis lanata, from southeastern Europe, provides digoxin, long used for heart failure and arrhythmia (Whayne, 2018).

In the current era, it is possible to screen a large number of compounds in silico via molecular docking and ADMET analysis (absorption, distribution, metabolism, excretion, and toxicity), which has made new drug discovery more efficient (Lionta et al., 2014). In this study, we constructed a library of 2792 natural compounds from 19 medicinal plants, many of which exhibit anticancer properties. We evaluated these compounds via molecular docking methods at the active site of the FLT3 protein to determine which compounds could bind tightly. Then, we analyzed the selected top compounds using the ADMET model and subjected them to laboratory-based testing in real-life biology studies via simulations to verify their potential safety and efficacy as medications. In our analysis, we identified several natural compounds that effectively inhibited FLT3 compared with conventional drugs. These results have the potential to open a new horizon in AML treatment.

2. MATERIALS AND METHODS

2.1. Protein preparation

The three-dimensional (3D) experimental tertiary protein structure of FMS-like tyrosine kinase 3 (FLT3, PDB ID Code: 6JQR), which is a drug target for our study, was obtained from the RCSB Protein Data Bank (PDB) in PDB format (Berman et al., 2000). The structure was resolved using X-ray diffraction at a high resolution of 2.20 Å (free R value: 0.213, observed R value: 0.181, and work R value: 0.179), with a molecular weight of 39.34 kDa (Amano, 2024; Kawase et al., 2019). From beginning to end, we prepared the target in BIOVIA Discovery Studio Visualizer 2024 software (BIOVIA, 2024) with all the metal ions, cofactors, and water molecules removed. Upon refining the protein structure, it underwent subsequent optimization, validation, and minimization via the GROMOS force field of the Swiss PDB Viewer (SPDV) v4.1.0. It was saved in PDB format (Guex et al., 2009).

2.2. Compounds retrieval and preparation

Phytocompounds are the chemical constituents contributing to the therapeutic effects of certain medicinal plants and formulations used for centuries for curing various diseases, and play an indispensable role in drug discovery. In this study, we used a curated database, namely, Indian Medicinal Plants, Phytochemistry and Therapeutics 2.0 (IMPPAT 2.0) (accessed on May 03, 2024, IMPPAT 2.0) (Vivek-Ananth et al., 2023). Keywords used were "*Azadirachta indica*", "*Bacopa monnieri*", "*Camellia sinensis*", "*Carthamus tinctorius*", "*Curcuma longa*", "*Ginkgo biloba*", "*Hypericum perforatum*", "*Moringa oleifera*", "*Mucuna pruriens*", "*Nigella sativa*", "*Origanum vulgare*", "*Panax ginseng*", "*Piper nigrum*", "*Psidium guajava*", "*Santalum album*", "*Withania somnifera*", "*Zingiber officinale*", "*Acorus calamus*", "*Aloe vera*", "phytochemical constituents", "bioactive compounds", and different combinations thereof to obtain the compounds. We collected 2792 compounds from 19 medicinal plants (**Fig. 1),** and excluded duplicate entries to maintain the accuracy of the dataset. The 3D structure and detailed information of each ligand were obtained from the PubChem database in SDF format (Kim et al., 2023). The compound library was prepared and optimized via OpenBabel software by energy minimization with the MMFF94 force field, and subsequently incorporating polar hydrogen atoms (O'Boyle et al., 2011). Finally, the ligands were merged into a single SDF file for ease of entry into the PyRx program (Dallakyan & Olson, 2015).

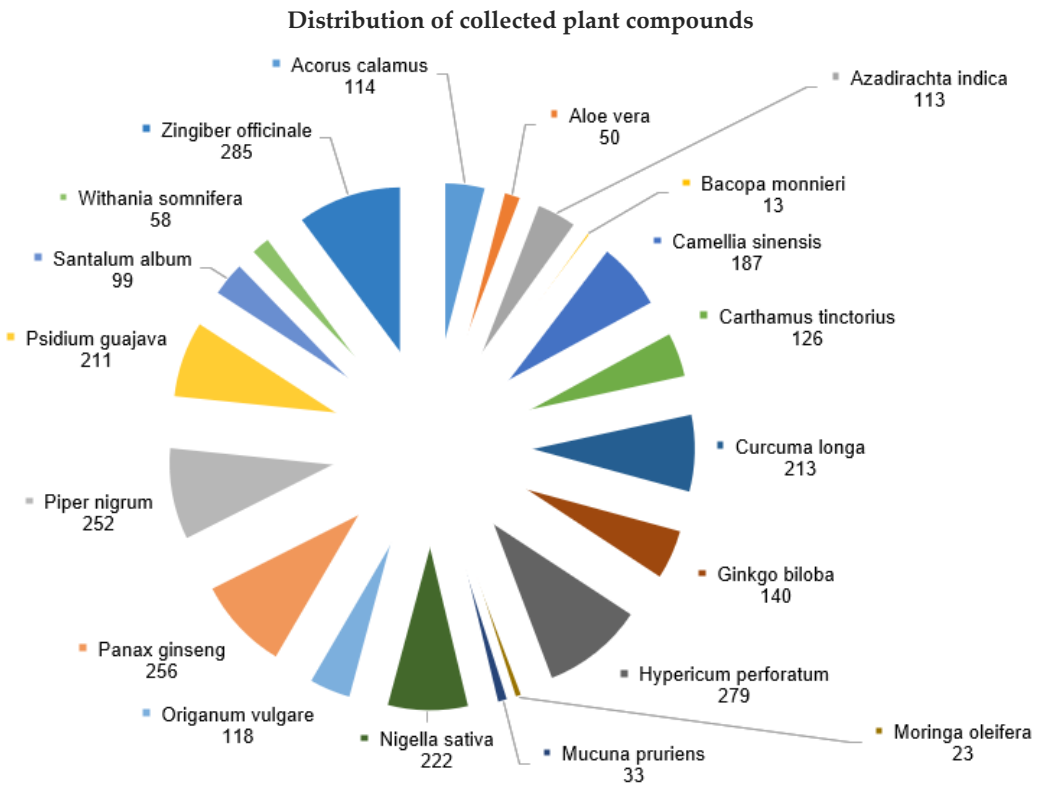

Fig. 1 The comparative distribution of compounds collected from 19 medicinal plants depicted in a radial bar chart. The segment size corresponds to the number of compounds collected, and a unique color distinguishes each plant species.

2.3. Grid generation and active site recognition

Discovery Studio was used to perform 6JQR analysis and establish the position of binding site residues. The receptor cavity recognized by Discovery Studio provides a reliable and comprehensive topological analysis of the protein. It allows the identification and quantification of binding site pocket residues, as well as the determination of volume, cavities, and channels. The server's prediction included many active pockets, and the initial binding site was identified based on its extensive surface coverage and size. To avoid blind docking, we used the receptor cavity in Discovery Studio and identified binding site residues to set up a grid box for virtual screening around the 6JQR protein (Atre et al., 2024). It is imperative to select the correctly predicted amino acid residue to ensure that the grid box in PyRx software encompasses the binding site of the target protein (Dallakyan & Olson, 2015).

2.4. Virtual screening

Structure-based virtual screening (VS) is a popular computational method in the early stages of drug design, discovery, and development. It is used by many pharmaceutical corporations and research teams (Razzaghi-Asl et al., 2018). This technique enables researchers to anticipate the best binding poses of a library of small compounds to specific macromolecules. PyRx 0.8 software is a dependable open-source VS program that is commonly used in CADD to screen vast libraries of compounds against an exact therapeutic target (Dallakyan & Olson, 2015). This study used PyRx's AutoDock Vina wizard to select compounds (n=2792) from 19 medicinal plants to identify potential anticancer drug candidates with significant activity against the FLT3 receptors in acute myeloid leukemia. We transformed each ligand into an AutoDock ligand, loaded the produced protein into PyRx, and then converted it to a dockable PDBQT file. Exhaustiveness value was 8, the default value. The grid box's center coordinates were X: −25.09, Y: −0.46, and Z: −20.70, with dimensions of X: 37.1900, Y: 25.7513, and Z: 21.0501 angstroms (Å) around the 6JQR protein. The top 15 candidates were selected for further pharmacokinetic testing upon ranking the compounds by binding affinity (with the most negative being the highest) and analyzing their docking poses. These poses allowed the compounds to engage with specific residues inside the binding

site of the target receptor protein. Finally, we used Discovery Studio (BIOVIA, 2024) to manually inspect the binding interactions of the protein-ligand complexes that scored the highest.

2.5. Pharmacokinetic property prediction

The rate and time course of drug entry and excretion in the body depend mainly on four processes — Absorption, Distribution, Metabolism, and Excretion — abbreviated as ADME. In this study, the pharmacokinetic (PK) and drug-likeness (DLP) properties of small molecular compounds were evaluated using the widely used system called SwissADME (Daina, Michielin & Zoete, 2017).

2.6. Toxicity investigation

The ability of a substance to harm living organisms or their parts, such as cells and organs, is called the toxicity of that substance. Drug development typically fails in later stages because of this issue, making toxicological profile inspection a key step (Wang et al., 2015). Currently, computer-aided in silico testing is being used to assess chemical toxicity, implying animal trials are no longer necessary. Potential anticancer agent cytotoxicity, hepatotoxicity, carcinogenicity, mutagenicity, and immunotoxicity were evaluated via the pkCSM (https://biosig.lab.uq.edu.au/pkcsm/prediction) (Pires, Blundell & Ascher, 2015) and ProTox 3.0 (tox.charite.de/protox3) prediction algorithms (Banerjee et al., 2024).

2.7. Molecular dynamics simulation

Molecular dynamics (MD) simulations provide valuable information about biological motion by observing the stability, structural changes, and variations of protein and ligand complex formations, which helps in the analysis of crucial physiological processes (Ja'afaru et al., 2024; Alhumaydhi et al., 2021). We ran four rounds of molecular dynamics (MD) simulations on three protein–ligand complexes and one control sample as a part of our investigation. The simulations were performed for up to 100 nanoseconds (ns) using the YASARA (version 24.4.10) dynamics software equipped with the Amber 14 force field (Krieger & Vriend, 2015; Wang et al., 2004). Upon cleaning and optimizing, including optimization of the hydrogen bond network, the docked complexes were centrally placed in a cubic simulation box, where periodic boundary conditions were applied, and solvated by TIP3P water molecules (Harrach & Drossel, 2014). The cubic box size was 80 × 80 × 80 Å, and the distance between the box edge and the protein edge was 12.5 Å. The simulation system was set to 310 K, pH 7.4, and NaCl concentration 0.9% to simulate physiological conditions. First, energy minimization was performed using the Swiss PDB viewer to optimize the structure and eliminate steric conflicts. To calculate long-range electrostatic interactions, the Particle Mesh Ewald (PME) method was used (Essmann et al., 1995) while the short-range interactions of van der Waals and Coulomb interactions were examined using a cutoff radius of 8 Å. The simulations were conducted at a constant temperature and pressure using a Berendsen thermostat. Trajectory data for analysis were saved every 250 ps (Akash et al., 2023a). Topology files for ligands are auto-generated using General AMBER Force Field (GAFF) and AM1BCC charges. We examined a variety of parameters to assess the conformational stability of both the apoprotein and complex systems. These parameters included: RMSD, RMSF, radius of gyration, SASA, and H-bond interactions (Genheden & Ryde, 2015).

3. RESULTS & DISCUSSION

3.1. Virtual screening-based molecular docking

Pharmaceutical research and development require knowledge of how small-molecule ligands recognize and interact with proteins. Molecular docking is one of the vital computational tool that allows scientists to analyze these binding processes. These include the process of ligand binding and the study of intermolecular interactions that help stabilize the ligand-receptor complex (Akash et al., 2023b). Owing to successful molecular docking between the previously predicted active region of the FMS-like tyrosine kinase 3 (FLT3) receptor protein and a library of 2792 phytochemicals, we determined that the binding affinity varied from −2.5 to −10.9 kcal/mol. We evaluated the pharmacokinetic properties of 256 compounds with their docking scores ranging between −8.9 and −10.9 (see supplementary file (**SM_1**)). Of these, the top 15 compounds showing the most favorable pharmacokinetic properties are presented in **Table 3**. In addition, **Table 1** summarizes their source, PubChem CID, compound name, binding affinity (kcal/mol), and average binding affinity. From this analysis, three were identified as the most promising lead candidates: Withanicandrin (−10.9 kcal/mol), 17Beta−Hydroxywithanolide K (−10.1 kcal/mol), and Asperglaucide (−9.4 kcal/mol). Compounds with binding energy lower than −6.0 kcal/mol are expected to exhibit activity against a protein (Chandra et al., 2022). Therefore, the higher binding affinities of these chosen compounds to our target protein, FLT3, indicate these compounds may show enhanced potency in ameliorating acute myeloid

leukemia (AML). Notably, gilteritinib (binding affinity of −9.1), an orally accessible small-molecule inhibitor of FMS-like tyrosine kinase 3, is administered to AML patients with FLT3 mutations. However, gilteritinib therapy has been associated with a modest increase in the incidence of serum aminotransferase, which can lead to acute liver injury and cause immunotoxicity.

Table 1: A catalog featuring the top 15 compounds, detailing their plant sources, PubChem CIDs, names, binding affinities (kcal/mol), and average values.

S.L. No.	Source	PubChem CID	Compound Name	Binding affinity (Kcal/mol)			Avg. binding affinity
				1st	2nd	3rd	
1	*Psidium guajava*	**91809632**	Withanicandrin	−10.9	−10.9	−10.9	−10.9
2	*Psidium guajava*	**44562998**	17Beta-Hydroxywithanolide K	−10.2	−10.2	−9.9	−10.1
3	*Panax ginseng*	5281629	6-Deoxyjacareubin	−9.9	−9.6	−9.6	−9.7
4	*Moringa oleifera*	**10026486**	Asperglaucide	−9.7	−9.2	−9.2	−9.4
5	*Panax ginseng*	72307	sesamin	−9.3	−9.3	−9.2	−9.3
6	*Ginkgo biloba*	520461	Epsilon-Muurolene	−9.2	−7.1	−7.1	−7.8
7	*Azadirachta indica*	11334829	Nimbidiol	−9.2	−9.2	−9.2	−9.2
8	*Carthamus tinctorius*	5458878	Nb-p-Coumaroyltryptamine	−9.2	−9.2	−9.2	−9.2
9	*Carthamus tinctorius*	5458879	N-Coumaroyl serotonin	−9.1	−9.0	−9.1	−9.1
10	*Azadirachta indica*	189403	12-Hydroxy-13-methylpodocarpa-8,11,13-triene-3,7-dione	−9.1	−9.2	−9.2	−9.2
11	*Ginkgo biloba*	5281624	6-(3,3-Dimethylallyl)-1,5-dihydroxyxanthone	−9.1	−9.0	−9.0	−9.0
12	*Carthamus tinctorius*	119205	Matairesinol	−9.0	−9.0	−8.9	−9.0
13	*Azadirachta indica*	11119228	Nimbiol	−9.0	−9.0	−9.0	−9.0
14	*Azadirachta indica*	189728	12-methyl-7-oxopodocarpa-8,11,13-triene-13-carboxylic acid	−9.0	−9.0	−9.0	−9.0
15	*Azadirachta indica*	189726	Margolonone	−9.0	−9.0	−9.0	−9.0
Standard FLT3 drugs							
1	Synthetic	49803313	Gilteritinib	−9.3	−8.9	−9.1	−9.1

3.1.1. Protein–ligand relations

The coordination of weak or covalent connections in protein-ligand complexes is the most vital aspect in the development of a new drug. Measuring bonding distance, binding site, and protein-ligand interactions provided valuable insight into the relationship between the compound and the protein (Tahamid Tusar et al., 2025). We visualized the ligand–protein docked complexes via the BIOVIA Discovery Studio Visualizer to increase comprehension of the intermolecular interactions between the selected compounds and the FLT3 monomer. The molecular interactions of the FLT3 monomer with the three most potent compounds and one control (existing drug)—Asperglaucide (CID:10026486), 17-beta-hydroxywithanoid K (CID: 44562998), withanicandrin (CID: 91809632), and gilteritinib (control) (CID: 49803313)—are presented, with the binding interaction patterns illustrated in both 2D and 3D formats in **Fig. 2** to **Fig. 3.** Based on our findings, every molecule exhibited a wide range of bonding and nonbonding interactions with residues at the binding site or nearby. The main features of the interaction between protein and ligand are van der Waals attraction, pi-donor hydrogen bonding, and general hydrogen bonding. Understanding how ligands attach to proteins relies on all of these factors. Here, the asperglaucide molecule forms two conventional hydrogen bonds with the MET837 amino acid located in chain A; for this, it uses the hydrogen atoms HN2 (2.69 Å) and HN3 (2.63 Å) of its amide group. These relatively short bond distances indicate that these are very strong and favorable interactions. In addition to hydrogen bonding, electrostatic pi-anion interactions occur with ASP 811 (3.71 Å), where the side chain of the aspartate amino acid attracts the electron-rich system (pi system) of asperglaucide. The binding interface is further stabilized by extensive hydrophobic interactions. The interface also engages in pi–pi stacking interactions with the aromatic residues PHE830 (3.78 Å), PHE621 (3.78 Å), and TYR842 (4.82 Å). Pi-alkyl interactions form with the aliphatic side chains of ALA620 (4.92 Å), ALA848 (5.39 Å), and ARG849 (5.12 Å), too, helping anchor the molecule in the binding site. This type of interaction can significantly

contribute to binding affinity and specificity. 17-Beta-Hydroxywithanoid K demonstrated one strong hydrogen bond (2.55 Å) between the ARG849 hydrogen and UNK1's (ligand) oxygen. Multiple hydrophobic interactions, including pi-sigma interactions with TYR842 (3.98 Å) and PHE621 (3.76 Å) and Pi-alkyl interactions with TYR572, PHE621, PHE830, and TYR842 (distances: 4.21–5.32 Å), have also been reported.

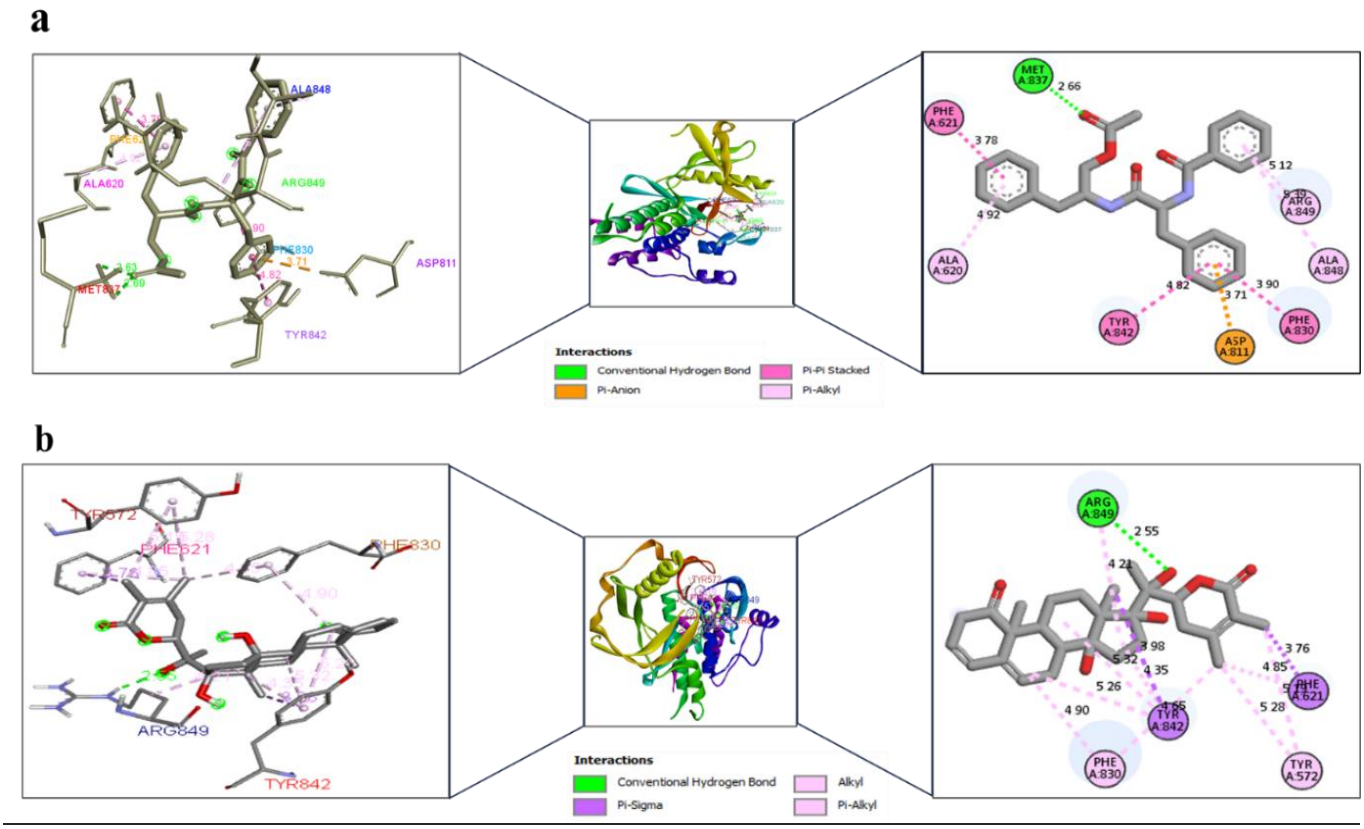

Fig. 2 Intermolecular interactions between the FLT3 receptor protein and (a) asperglaucide and (b) 17-beta-hydroxywithanoid K, showing the binding pose (middle), 3D binding interaction patterns (left), and 2D interaction patterns (right).

Conversely, withanicandrin contributed to the establishment of three hydrogen bonds with protein residues, including two strong bonds with GLN575 (2.36 Å and 3.08 Å) and one very short bond with ARG849 (2.28 Å), pointing to highly favorable polar interactions. Additionally, a hydrophobic alkyl interaction occurs between ARG849 and UNK1 (withanicandrin) (4.34 Å). The ligand gilteritinib (control) interacts with the protein target through weak interactions, suggesting suboptimal binding characteristics. ASP811, PHE830, and GLU573 form three carbon-hydrogen bonds, but their distances (3.31–3.52 Å) are beyond the ideal range for strong hydrogen bond formation. The hydrophobic interactions are predominantly weak, with pi-sigma and pi-pi stacking only close to the upper limit of the optimal distance. The only intermediate stabilizing interaction is a pi-alkyl contact with ARG849 (3.89 Å). This pattern suggests that binding may be transient or low-affinity, and that stronger interactions are needed to improve stability and binding affinity.

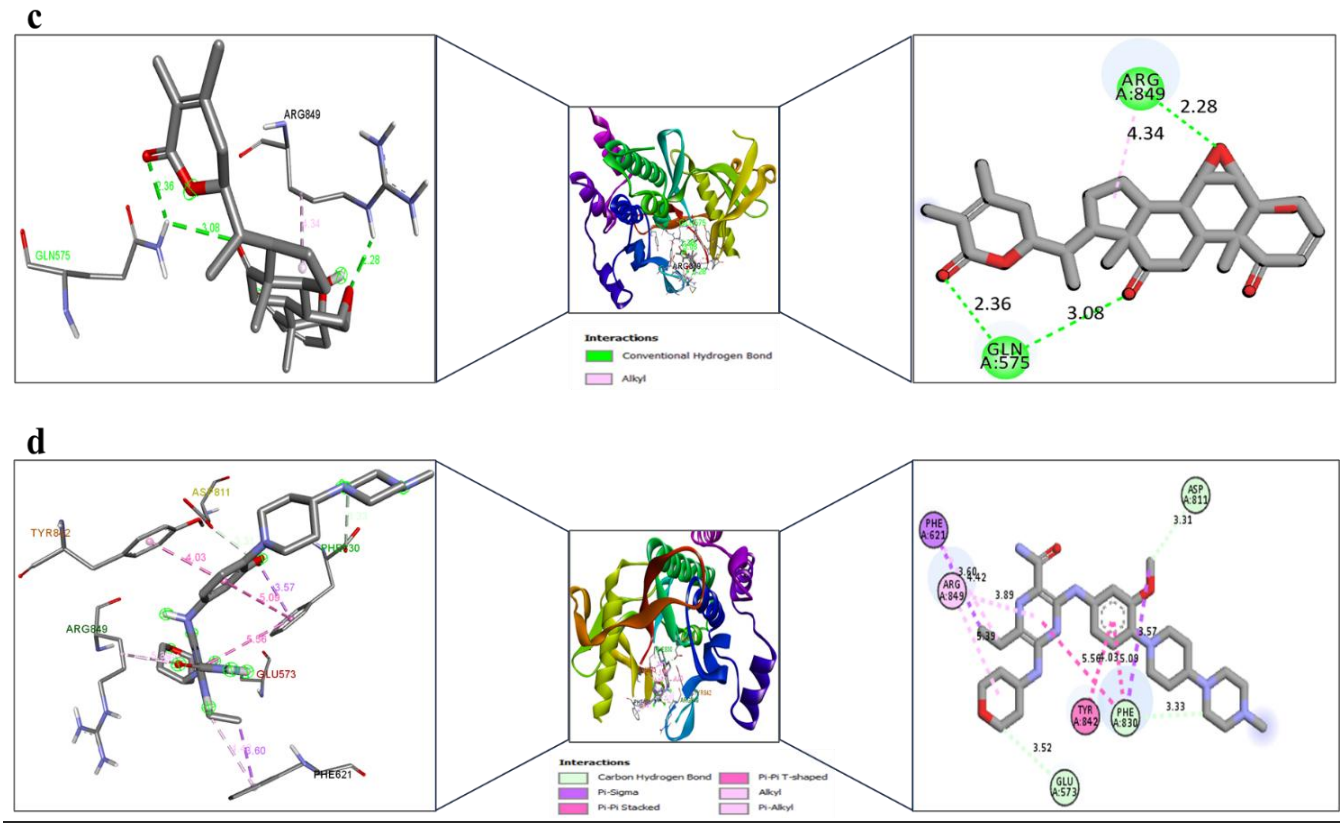

Fig. 3 Intermolecular interactions between the FLT3 receptor protein and (c) withanicandrin and (d) gilteritinib, showing the binding pose (middle), 3D binding interaction patterns (left), and 2D interaction patterns (right).

In our analysis, all the selected ligands formed interactions with the FLT3 protein primarily via hydrogen bonds. **Fig.4** shows the regions involved in hydrogen bond donation and acceptance during the three-dimensional interactions between the FLT3 protein and the three best-selected compounds and one existing drug (control). Hydrogen bonds play an indispensable role in defining the strength and specificity of the interaction between a protein and its ligand. As shown in **Table 2**, analysis revealed that all the ligands also had strong hydrophobic interactions with the FLT3 receptor.

Table 2: Intermolecular contacts between the FLT3 protein and bound ligands.

Compound	Interaction Type	Residue(s)	Details (Distance in Å)
Asperglaucide	Hydrogen Bond	MET837 (Chain A)	HN2 – 2.69 Å, HN3 – 2.63 Å
	Electrostatic (P-Anion)	ASP811	3.71 Å
	Pi-Pi Stacking	PHE830, PHE621, TYR842	3.78 Å, 3.78 Å, 4.82 Å
	Pi-Alkyl	ALA620, ALA848, ARG849	4.92 Å, 5.39 Å, 5.12 Å
17-Beta-Hydroxywithanoid K	Hydrogen Bond	ARG849 – UNK1 (oxygen)	2.55 Å
	Pi-Sigma	TYR842, PHE621	3.98 Å, 3.76 Å
	Pi-Alkyl	TYR572, PHE621, PHE830, TYR842	4.21–5.32 Å
Withanicandrin	Hydrogen Bond	GLN575, ARG849	2.36 Å, 3.08 Å, 2.28 Å
	Alkyl (Hydrophobic)	ARG849 – UNK1	4.34 Å
Gilteritinib (Control)	Carbon–Hydrogen Bond	ASP811, PHE830, GLU573	3.31–3.52 Å
	Pi-Sigma/Pi-Pi Stacking	General (weak)	At the upper limits of favorable distances
	Pi-Alkyl	ARG849	3.89 Å

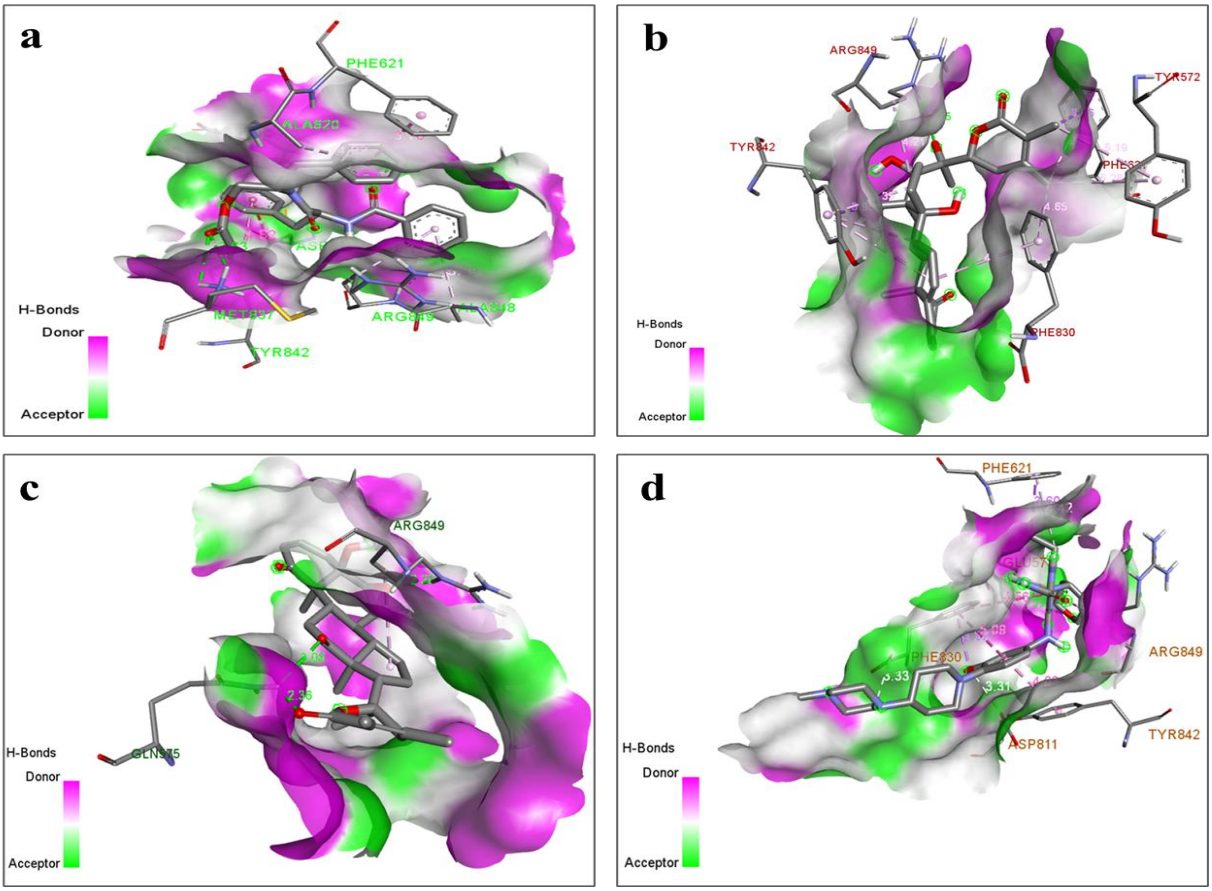

Fig. 4 Areas engaged in hydrogen bond donation and acceptance throughout the three-dimensional interactions between the FLT3 protein and the three best-selected compounds and one existing drug: (a) asperglaucide, (b) 17-beta-hydroxywithanoid K, (c) withanicandrin, and (d) gilteritinib (control).

3.2. ADME properties

Conducting in silico pharmacokinetic analysis is essential in modern drug discovery because it allows for the evaluation of the physicochemical characteristics of candidate compounds while saving time and money (Islam et al., 2024). The pharmacokinetic analyses via SwissADME revealed that the pharmacokinetic and pharmacodynamic properties of the top 256 compounds were analyzed after molecular docking, as detailed in the Supplementary file (**SM_2**). Assessing the pharmacokinetic properties of the top 15 compounds considering their physicochemical characteristics, water solubility, lipophilicity, pharmacokinetics, drug-likeness, and medicinal chemistry, allowed determining their suitability as drug candidates (**Table 3)**. The evaluation revealed that all the compounds fully adhered to Lipinski's rule of five except for the control, suggesting significant potential for oral bioavailability (Lipinski, Dominy & Feeney, 1997). The compounds were all considered having adequate bioavailability because they had molecular weights less than 500 g/mol, an acceptable number of hydrogen bond donors (ranging from 0 to −3), and a moderate number of acceptors (ranging from 2 to −6). Additionally, they all included between 1 and 13 rotatable bonds. The ideal range for effective membrane permeability was 2.03 to −3.73 for the log Po/w (iLOGP) values. The water solubilities of the compounds ranged from −3.52 to −5.0, with the majority being moderately to highly soluble in biological settings, according to the Log S (ESOL) values.

High gastrointestinal (GI) absorption was predicted for all compounds, suggesting that they would be suitable for oral drug formulations. Nine compounds that were not our primary focus showed evidence of the ability to cross the blood-brain barrier (BBB). The synthetic accessibility scores of these compounds ranged from 2.43 to −6.45, suggesting that their synthesis was primarily moderately complicated. Other drug-likeness criteria, such as the Ghose, Veber, Egan, and Muegge standards, were effectively met for most compounds, with no violations (details not mentioned). However, some compounds, such as CID: 10026486, CID: 91809632, and CID: 44562998, showed relatively high synthetic accessibility scores, suggesting relatively high synthesis complexity. Among all the candidates, CID: 10026486, CID: 91809632, and CID: 44562998 were identified as the most promising, as they exhibited favorable

pharmacokinetic properties. These compounds did not show any Lipinski violations, exhibited moderate Log Po/w (iLOGP) values (3.49, 3.33, and 3.73, respectively), satisfactory aqueous solubility (Log S) values (−4.5 and −4.1), and synthetic accessibility scores (3.31, 6.45, and 6.65, respectively). Despite neither molecule being permeable to the blood-brain barrier, their superior gastrointestinal absorption and adherence to drug-likeness criteria render them compelling candidates for further exploration. For reference, the standard FLT3 inhibitor gilteritinib (CID: 49803313) demonstrated a higher molecular weight (552.71 g/mol) and two Lipinski violations, along with a Log S value of −5.08, showing comparatively lower solubility and slight deviations from ideal drug-like properties.

Table 3: Analysis of the drug-likeness and pharmacokinetic properties of 15 compounds identified via the SwissADME server.

Properties			Physiochemical properties					Lipophilicity	Water solubility	Pharmacokinetics		Druglikeness	Medical chemistry
Parameters		MW (g/mol)	Heavy atoms	Arom. Heavy atoms	Rotatable bonds	H–bond acceptors	H–bond donors	Log Po/w (iLOGP)	Log S(ESOL)	GI absorption	BBB permeant	Lipinski	Synthetic accessibility
S.L	CID												
1	**10026486**	**444.52**	**33**	**18**	**13**	**4**	**2**	**3.49**	**−4.95**	**High**	**No**	**Yes; 0 violation**	**3.65**
2	119205	358.39	26	12	6	6	2	2.47	−4.06	High	No	Yes; 0 violation	3.3
3	5281629	310.30	23	14	0	5	2	2.93	−4.56	High	No	Yes; 0 violation	3.57
4	72307	354.35	26	12	2	6	0	3.46	−3.93	High	Yes	Yes; 0 violation	4.12
5	520461	354.35	26	12	2	6	0	3.46	−3.93	High	Yes	Yes; 0 violation	4.12
6	**91809632**	**468.58**	**34**	**0**	**2**	**6**	**1**	**3.33**	**−4.5**	**High**	**No**	**Yes; 0 violation**	**6.31**
7	**44562998**	**470.60**	**34**	**0**	**2**	**6**	**3**	**3.73**	**−4.1**	**High**	**No**	**Yes; 0 violation**	**6.45**
8	11334829	274.35	20	6	0	3	2	2.14	−4.37	High	Yes	Yes; 0 violation	3.13
9	189403	286.37	21	6	0	3	1	2.36	−3.72	High	Yes	Yes; 0 violation	3.15
10	11119228	272.38	20	6	0	2	1	2.86	−4.81	High	Yes	Yes; 0 violation	3.16
11	189728	300.39	22	6	1	3	1	2.43	−4.82	High	Yes	Yes; 0 violation	3.35
12	189726	314.38	23	6	1	4	1	2.03	−3.74	High	Yes	Yes; 0 violation	3.34
13	5281629	310.30	23	14	0	5	2	2.93	−4.56	High	No	Yes; 0 violation	3.57
14	5281624	296.32	22	14	2	4	2	3.1	−5	High	Yes	Yes; 0 violation	3.19

15	5458878	306.36	23	15	6	2	3	2.21	−3.52	High	Yes	Yes; 0 violation	2.43
Standard FLT3 drugs													
1	49803313 (Gilteritinib)	552.71	40	12	9	7	4	4.15	−5.08	High	No	No; 2 violations	4.73

3.3. Toxicological evaluation

Detrimental side effects are one of the leading causes of drug development failure in the early stage, and drug toxicity is a key concern in the medical industry (Lipinski et al., 2001). The degree to which a chemical may damage living things or their constituent parts, such as cells and organs, is called its toxicity. Therefore, early identification of toxicity is highly beneficial (Lagorce et al., 2017). We analyzed the toxicological properties of 256 compounds (see supplementary file **SM_3**); **Table 4** highlights potential toxicity outcomes of all the examined molecules. Among the compounds evaluated, asperopleaucide (CID: 10026486) is noteworthy. Asperopleaucide selectively inhibits hERG II, which has potential cardiovascular applications. Its ORAT value (1.961) is within the acceptable range, suggesting its acute toxicity is tolerable. It is free of hepatotoxicity, carcinogenicity, immunotoxicity, and mutagenicity. Its maximum tolerated dose (MTD) is −0.541, suggesting better tolerability than the other plant compounds used in this study. 17Beta-hydroxywithanolide K (CID: 44562998) is similarly promising, as it has an entirely safe toxicity profile. This compound did not yield negative results in any toxicity test, including AMES, hepatotoxicity, and mutagenicity. Although its MTD (−0.701) is slightly lower than that of asperopleaucide, its overall safety profile makes it ideal for situations where few side effects are common. These plant compounds have shown better safety profiles than the reference drug gilteritinib, which is known for the induction of immunotoxicity (Dugan et al., 2021). Although withanicandrin is nontoxic, its low MTD value (−0.797) limits its potential. For this reason, this compound is still a potential drug candidate.

Table 4: Evaluation of the toxicity profiles induced by the three potential hit molecules and standard FLT3 drugs.

Compound CID	Phytochemical Name	pkCSM						ProTox			
		AMES toxicity	MTD	hERG I inhibitor	hERG II inhibitor	ORAT	SS	Hepatotoxicity	Carcinogenicity	Immunotoxicity	Mutagenicity
10026486	Asperglaucide	No	−0.541	No	Yes	1.961	No	Inactive 0.70	Inactive 0.66	Inactive 0.99	Inactive 0.70
44562998	17Beta−Hydroxy withanolide K	No	−0.701	No	No	2.3	No	Inactive 0.88	Inactive 0.52	Inactive 0.54	Inactive 0.88
91809632	withanicandrin	No	−0.797	No	No	2.873	No	Inactive 0.79	Active 0.57	Active 0.99	Inactive 0.72
Standard FLT3 drugs											
49803313	Gilteritinib	No	−0.112	No	Yes	2.429	No	Inactive 0.61	Inactive 0.59	Active 0.80	Inactive 0.58

3.4. Molecular dynamics simulation

To test their dynamic insight, stability, and binding pocket for proteins at the atomic level, which provides insights for drug discovery, molecular dynamics simulations were performed for 100 ns of the four compounds. This study used several evaluation metrics collected from MD trajectory data, such as Root Mean Square Deviation (RMSD), Root Mean Square Fluctuation (RMSF), Hydrogen Bonding Count, Solvent Accessible Surface Area (SASA), and Radius of Gyration (RG).

3.4.1. RMSD

We performed root mean square deviation (RMSD) analysis of the molecular dynamics simulation, which revealed insights into the structural stability, conformational dynamics, and protein binding ability of the studied systems. The RMSD plots of three test

compounds, CID 10026486 (Asperglaucide), CID 44562998 (17Beta-Hydroxywithanolide K), and CID 91809632 (Withanicandrin), were observed to measure their atomic position deviations from the initial reference structure. In this analysis, shown in **Fig. 5**, the X-axis specifies time (0 to 100 ns), which displays the progress of the simulation. On the other hand, the Y-axis expresses the RMSD (0.5 to 2.5 Å), which provides a quantitative value of the positional change of the atoms with respect to the initial reference structure. In the MD simulation, a constant RMSD value with slight variation confirms a converged system. High RMSD fluctuation typically means that the ligand loses its strong interaction integrity with the protein and that the protein's binding site shifts or leaves the binding pocket. In contrast, low fluctuation means that the protein's binding pocket is relatively stable. Moreover, a lower RMSD value indicates that the ligand remains compatible with the binding site and maintains a more stable conformation within the binding pocket over time, whereas a higher RMSD value implies that the ligand–protein combination has poorer stability and a weaker binding affinity (Hollingsworth & Dror, 2018; Stumpfe, Geppert & Bajorath, 2010).

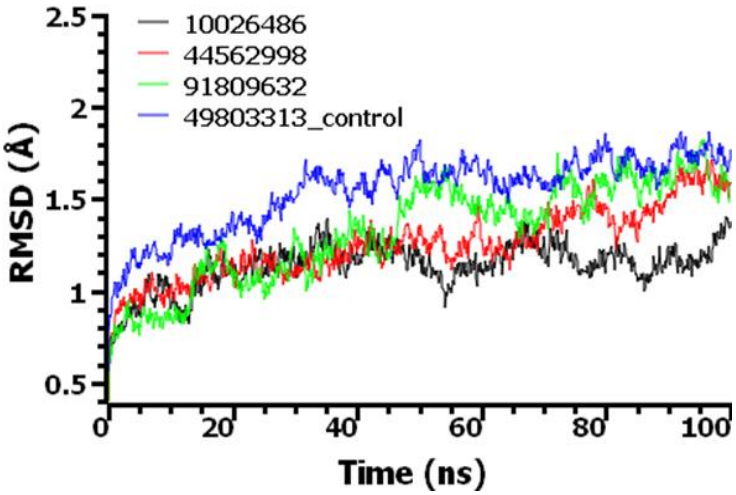

Fig. 5 Root mean square deviation (RMSD) trajectories (in Ångströms) of three experimental samples, 10026486 (black), 44562998 (red), 91809632 (green), and the control system 49803313 (blue), over the simulation time (100 ns).

All the samples presented comparably low RMSD values, ranging from 0.403 to 0.559 nm, indicating stable initial structures. However, the control CID:49803313 (gilteritinib) began with a slightly higher RMSD than the experimental sets did, signifying detrimental starting compatibility or greater preequilibrium with the target protein. Throughout the simulation, the control path showed a slowly increasing RMSD, with a high point of 1.36 Å at 14 ns, followed by a temporary decrease and recovery to 1.54 Å at 26.2 ns. Even though it converged at 1.39 Å at 27.8 ns, this fluctuation may indicate movement into or out of the binding pocket or temporary instability. Furthermore, a noticeable peak at 1.82 Å at 50 ns and the largest RMSD of 1.87 Å at 92 ns hint at long-term conformational drifts linked to weakened ligand-protein interactions. Overall, the control group exhibited weak to moderate binding affinity and dynamic instability in the binding pocket, indicated by a high average RMSD value of 1.541 Å, although it reached a plateau phase in the later stages of the simulation. **Table 5** depicts the mean values of different samples and the control. Withanicandrin had a more stable RMSD profile with an average value of 1.326 Å. However, it exhibited considerable deviations at 12.2 ns (0.82–1.27 Å), 44.9 ns (1.17–1.63 Å), and 66.5 ns (1.31–1.75 Å); these deviations preceded recovery and stabilization tendencies, indicating dynamic flexibility in the binding site. The maximum observed deviation of 1.82 Å at 95.8 ns is within the framework of transient behavior and not of continual instability, reminiscent of a general moderate to strong binding profile with occasional conformational fluctuations. Asperglaucide had auspicious outcomes. The lowest average RMSD value for all the compounds was 1.14 Å, and the peak decreased to 0.903 Å at 54.2 ns, followed by a consistent increase to a plateau of 1.37 Å at approximately 67.4 ns and a consistent decrease to a value of roughly 1 Å at 86.2 ns, suggesting the reclamation of a stable conformation. These results demonstrate a high capacity for readjustment and a generally stable connection with the protein. 17 Beta–hydroxywithanolide K also exhibited relatively low fluctuations, with an overall average RMSD of 1.25 Å and a stable path until the first 50 ns; this ligand continued to possess better conformational stability in the binding pocket. Slight deviations followed after 50 ns at 57.6 ns, 67.9 ns, and 83.3 ns, but were within acceptable values with recovery. The RMSD was well within its minimum (0.401 Å) and maximum (1.715 Å) values, so

there were uniform binding interactions with minimal disturbance, suggesting improved affinity and structural fit. Regarding binding site stability, structural stability, and interaction resistance, all the experimental ligands outperformed the control, according to the combined RMSD data. Of these compounds, asperglaucide was the most stable and promising candidate. It was observed to have high binding affinity, a stable equilibrium, and negligible variation.

3.4.2. RMSF analysis

Root Mean Square Fluctuation (RMSF) is a measurement method used to analyze the local dynamics or movements of amino acid residues and ligand atoms in proteins at different temperatures and pressures. It is beneficial in determining individual atom flexibility and provides information about ligand binding, which affects the structural flexibility of the entire protein. Higher RMSF values indicate greater flexibility and potential destabilization, whereas lower values indicate reduced motion and greater stability of the protein-ligand complex (Song et al., 2024). The RMSF values of the control gilteritinib (blue) and the experimental ligands asperglaucide (black), 17beta−hydroxywithanolide K (orange), and withanicandrin (green) were confirmed. RMSF value, plotted on the y-axis in **Fig. 6(a),** is suggestive of the degree of atomic fluctuation and is expressed in units of angstroms (Å). Residues 571 to 951 are on the x-axis, matching the protein's amino acid sequence. The evaluation of local flexibility across the protein's terminal regions is made possible by this range, which extends from the N-terminal region (near residue 571) to the C-terminal region (near residue 951). **Fig. 6(a)** shows that among the four systems analyzed, the lowest mean RMSF of 0.944 Å and standard deviation of 0.375 Å were shown by asperglaucide, indicating that it gives the protein the maximum structural stability. In this compound, residue 651 (2.723 Å) fluctuated the most, followed by residues 624 (1.960 Å), 654 (1.954 Å), 618 (1.935 Å), and 622 (1.923 Å). These residues most likely live in loop sections or segments exposed to the surface, which maintain some mobility even when the protein is ligand−bound, although with less fluctuation than in the unbound state. A mild increase in flexibility is observed in the compound 17Beta-hydroxywithanolide K, as demonstrated by a slightly higher average RMSF of 1.020 Å with a standard deviation of 0.421 Å. 651 (2.678 Å), 781 (2.593 Å), 633 (2.454 Å), 608 (2.289 Å), and 630 (2.222 Å) are the most frequently fluctuating residues in this system. They suggest regions of the protein that might change their conformation in response to ligand interactions, which could impact binding-induced fit processes. A comparable average RMSF (Table 05) of 1.010 Å and a standard deviation of 0.406 Å were also shown by Withanicandrin, which had the most mobile residues at 781 (2.635 Å), 651 (2.412 Å), 633 (2.313 Å), 630 (2.192 Å), and 571 (1.991 Å). These high-fluctuation locations that overlap with 17Beta−Hydroxywithanolide K, Withanicandrin complexes suggest these areas are crucial for allosteric transitions or ligand engagement and are structurally sensitive. On the other hand, the highest RMSF value of 2.791 Å, the mean value of 0.992 Å, and the highest standard deviation of 0.430 Å were recorded for the control compound gilteritinib, all of which were located at residue number 651. This shows that the absence of ligand binding, especially in areas frequently thought to be the most mobile, leads to greater flexibility, such as residues 571, 633, 651, 652, and 781. Larger conformational variation and higher entropy within terminal areas are made possible by these intensified fluctuations, which point to a lack of stabilizing connections in the unbound state. According to a thorough RMSF investigation, ligand binding stabilizes the overall protein structure by reducing the amplitude of fluctuation in important dynamic areas in all four systems. With the largest RMSF of each system, residue 651 is a crucial hotspot of flexibility and is therefore a possible target location for ligand-induced stabilization. Other residues, such as residues 781, 633, and 630, also frequently fluctuate, suggesting that they might be components of a functional site or flexible domain that ligands influence.

3.4.3. Rg analysis

A structural characteristic called the radius of gyration (Rg) measures how compact a macromolecule, such as a protein or polymer, is overall. Rg is frequently used to evaluate the folding behavior, conformational stability, and structural alterations of biomolecules over time. Low Rg value indicates: The molecule is globular, compact, or firmly folded. Also, these findings imply robust intramolecular connections and structural stability and appropriate folding (in globular proteins). A high Rg score indicates the molecule is stretched, loosely packed, or partially unfurled(Newcomer, Lewis & Quiocho, 1981; Hong & Lei, 2008). As shown in **Fig. 6(b)**, the RG graph tracks signal responses for three ligand samples and one control across a 100 ns time span at 0.1 ns intervals, providing a comparative investigation of ligand-protein interactions. The 1001 data points in each data set reveal high temporal. All the ligand samples showed consistent signal patterns over time that closely resembled those of the control. According to the data, the control gilteritinib had the highest mean response (19.761 Å), followed by asperide (19.574 Å), 17Beta-hydroxywithanolide K (19.646 Å), and withanicandrin (19.709 Å). The ligand was highly stable, as illustrated by the continuously low standard deviations of 0.078 Å (Control), 0.072 Å (Withanicandrin), 0.061 Å (17Beta-hydroxywithanolide K), and 0.073 Å (Asperglaucide). To further support the consistency of the

interactions, the response range was tight for all samples, with values ranging from 0.380 Å to 0.464 Å. In terms of average signal and dynamic behavior, withanicandrin prominently showed the closest alignment to the control, implying that the compound caused a conformational or interaction state most akin to the native protein.

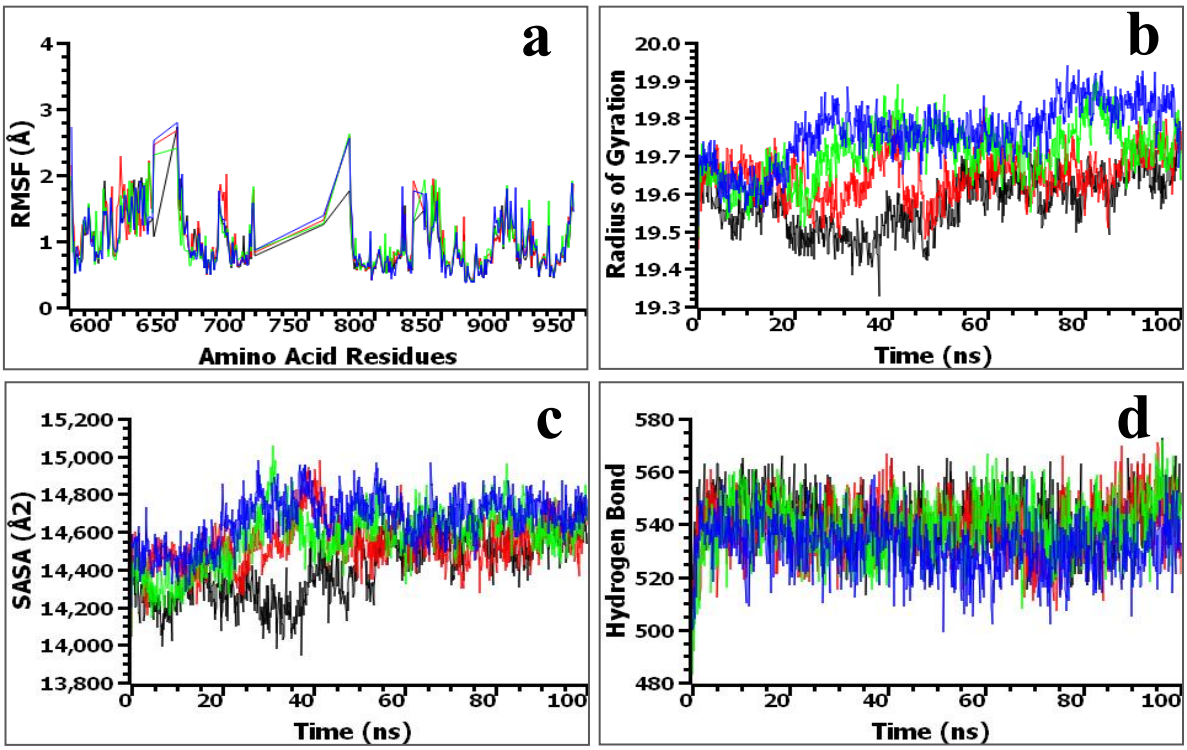

Fig. 6 Analysis of (a) root mean square fluctuations, (b) radius of gyration, (c) solvent accessible surface area, and (d) hydrogen bonds of asperglaucide, 17-beta-hydroxywithanolide K, withanicandrin, and the control based on a 100 ns MD simulation.

3.4.4. SASA analysis

Solvent accessible surface area (SASA) measures the exposed surface area of a molecule that is accessible to solvent molecules. SASA provides insight into the level of solvent exposure and the interactions that occur between a biomolecule and its surroundings. Fluctuations in SASA denote dynamic changes in protein folding or unfolding, ligand binding or unbinding, and overall protein-ligand interaction. For example, an increase in SASA can imply a protein complex unfolding and an increase in the available surface area of the protein complex. We summarized the results of all five analyses (RMSD (Å), RMSF (Å), Rg (Å), SASA (Å²), and H–Bond) in Table 5. As seen in Fig. 6(c), the average SASA of our test samples was marginally lower than that of Gilteritinib, suggesting a degree of structural compaction or decreased solvent exposure because of the samples being bound to their ligand. We also noticed that there are no abrupt changes or frequent strong downtrends in SASA, implying ligand binding or protein structural compaction, with less surface area exposed to the solvent. We did not find any abrupt changes or strong trends in the SASA curves for any of the four compounds, confirming the simulation's structural stability. Notably, 17Beta-Hydroxywithanolide K showed the least volatility over time, suggesting that it is the most stable and securely bonded complex. Asperglaucide on the other hand exhibited increased variance, which may indicate partial exposure or temporary structural changes.

3.4.5. Hydrogen bond analysis

Hydrogen bond analysis provided insight into the stability and intermolecular and intramolecular interactions of biomolecules, and the results are shown in **Fig. 6(d)**. Our analysis revealed that hydrogen bonds formed before the simulation stage, as all the experimental compounds (Asperglaucide, 17Beta-Hydroxywithanolide K, and Withanicandrin) and the control (Gilteritinib) hydrogen bond values increased by the 15 ns mark. This indicates that the ligand created complementarity of its binding pocket for the target protein and made stable interactions. The results also suggest that, in the middle stage of the simulation (40–60 ns), the bond values slightly decreased, suggesting that both ligand destabilization has occurred and the ligand moved out of the binding pocket, resulting in a low

interaction of the ligand–protein complex. The rest of the simulation time maintains a stable hydrogen bonding pattern for all the ligands. The mean values of the experimental samples are 542.46 (Asperglaucide), 538.87 (17Beta–Hydroxywithanolide K), 538.58 (Withanicandrin), and 531.57 (Gilteritinib). Asperglaucide has the highest mean value, indicating that this ligand is more stable and has the highest binding potential compared with the other two experimental ligands and the control.

Table 5: Summarizing the mean values of the control (49803313) and the three experimental samples (10026486, 44562998, 91809632) for the five analyses, RMSD (Å), RMSF (Å), Rg (Å), SASA (Å²), and H–Bond.

Analysis	10026486 (Asperglaucide)	44562998 (17Beta–Hydroxywithanolide K)	91809632 (Withanicandrin)	Control 49803313 (Gilteritinib)
RMSD (Å)	1.135	1.252	1.326	1.541
RMSF (Å)	0.944	1.020	1.010	0.992
Rg (Å)	19.574	19.646	19.709	19.761
SASA (Å²)	14.411	14.540	14.575	14.665
H–Bond	542.46	538.87	538.58	531.57

4. CONCLUSION

The main objective of our study was to explore the potential of natural compounds as FLT3 inhibitors in the treatment of acute myeloid leukemia (AML). Considering the side effects and drug resistance issues associated with current FLT3 inhibitors, such as gilteritinib, we constructed a library of 2792 natural compounds collected from 19 medicinal plants. We identified three compounds — asperglaucide, 17beta-hydroxywithanolide K, and withanicandrin — as the most promising FLT3 inhibitors using molecular docking, ADMET analysis, and 100-nanosecond molecular dynamics simulations. The efficacy and safety of the drugs were verified using a combination of molecular docking, ADMET analysis, and molecular dynamics (MD) simulations. Toxicity assessments conducted using ProTox and pkCSM platforms showed these compounds were nontoxic and did not exhibit hepatotoxic, mutagenic, or carcinogenic effects. In addition, SwissADME analysis exposed that all three compounds had high gastrointestinal absorption, indicating their oral bioavailability and potential for therapeutic application. Our study results suggest that asperglaucide and two compounds could be used as alternative FLT3 inhibitors for the treatment of AML. However, further in vitro and in vivo studies are needed to confirm the efficacy and safe use of these compounds. This study may open a new horizon in the treatment of AML, especially where current drugs have limitations.

Abbreviation	Full form
AML	Acute Myeloid Leukemia
FLT3	FMS-like tyrosine kinase 3
RCSB PDB	Research Collaboratory for Structural Bioinformatics Protein Data Bank
VS	Virtual Screening
ADME	Absorption, Distribution, Metabolism, and Excretion
PDBQT	Protein Data Bank, Partial Charge (Q), & Atom Type (T)
SDF	Structured Data File
RMSD	Root Mean Square Deviation
RMSF	Root Mean Square Fluctuation
Rg	Radius of gyration
SASA	Solvent Accessible Surface Area

Acknowledgements

The authors express their sincere gratitude to the Department of Biotechnology and Genetic Engineering, Faculty of Life Sciences, Gopalganj Science and Technology University-8100, Bangladesh, which provided generous support in implementing the computational research and provided all the necessary resources for the successful completion of the study

Authors' Contributions

Zubaer Hossen: Writing – original draft, Visualization, Validation, Methodology, Investigation. Md Rezoanul Islam: Methodology, Investigation, Md Sajjad Hossain: Methodology, Formal analysis, Data curation. Md. Naim Uddin Forhad: Graphical abstract, Methodology, Formal analysis, Investigation. Md Raichul Islam: Formal analysis, Data curation. Abdullah-Al-Jubayer: review & editing. Asura Khanam Lisa: review & editing. Md. Faruk Hasan: review & editing, software. Md. Enamul Haque: review & editing, supervision, & Conceptualization.

Ethical Approval

Not applicable.

Informed Consent

Not applicable.

Conflicts of interests

The authors declare that they have no known competing financial interests or personal relationships that could have influenced the work reported in this paper.

Funding

This research did not receive any specific grant from funding agencies in the public, commercial, or nonprofit sectors.

Data and materials availability

The processed data are available from the corresponding author & first author upon request.

REFERENCES

1. Abbas HA, Alfayez M, Kadia T, Ravandi-Kashani F, Daver N. Midostaurin in acute myeloid leukemia: An evidence-based review and patient selection. Cancer Manag Res 2019;11:8817–8828; doi: 10.2147/CMAR.S177894.
2. Akash S, Abdelkrim G, Bayil I, Hosen ME, Mukerjee N, Shater AF, Saleh FM, Albadrani GM, Al-Ghadi MQ, Abdel-Daim MM, Tok TT. Antimalarial drug discovery against malaria parasites through haplopine modification: An advanced computational approach. J Cell Mol Med. 2023;27(20):3168-3188. doi: 10.1111/jcmm.17940.
3. Akash S, Hosen ME, Mahmood S, Supti SJ, Kumer A, Sultana S, Jannat S, Bayıl I, Nafidi HA, Jardan YAB, Mekonnen AB, Bourhia M. Anti-parasitic drug discovery against Babesia microti by natural compounds: an extensive computational drug design approach. Front Cell Infect Microbiol. 2023 Aug 16;13:1222913. doi: 10.3389/fcimb.2023.1222913.
4. Alhumaydhi FA, Aljasir MA, Aljohani ASM, Alsagaby SA, Alwashmi ASS, Shahwan M, Hassan MI, Islam A, Shamsi A. Probing the interaction of memantine, an important Alzheimer's drug, with human serum albumin: In silico and in vitro approach. J Mol Liq 2021;340:116888; doi: 10.1016/J.MOLLIQ.2021.116888.
5. Atre I, Hollander-Cohen L, Lankry H, Levavi-Sivan B. Receptor cavity-based screening reveals potential allosteric modulators of gonadotropin receptors in carp (Cyprinus carpio). Computational and Structural Biotechnology Reports 2024;1:100026; doi: 10.1016/J.CSBR.2024.100026.
6. Banerjee P, Kemmler E, Dunkel M, Preissner R. ProTox 3.0: a webserver for the prediction of toxicity of chemicals. Nucleic Acids Res 2024;52(W1):W513–W520; doi: 10.1093/NAR/GKAE303.
7. Berman HM, Westbrook J, Feng Z, Gilliland G, Bhat TN, Weissig H, Shindyalov IN, Bourne PE. The Protein Data Bank. Nucleic Acids Res 2000;28(1):235–242; doi: 10.1093/NAR/28.1.235.
8. BIOVIA. Dassault Systèmes. Discovery Studio Visualizer, 2024
9. Chandra A, Chaudhary M, Qamar I, Singh N, Nain V. In silico identification and validation of natural antiviral compounds as potential inhibitors of SARS-CoV-2 methyltransferase. J Biomol Struct Dyn. 2022;40(14):6534-6544. doi: 10.1080/07391102.2021.1886174.
10. Daina A, Michielin O, Zoete V. SwissADME: A free web tool to evaluate pharmacokinetics, drug-likeness and medicinal chemistry friendliness of small molecules. Sci Rep 2017;7(1):1–13.
11. Dallakyan S, Olson AJ. Small-Molecule Library Screening by Docking with PyRx. Methods in Molecular Biology 2015;1263:243–250; doi: 10.1007/978-1-4939-2269-7_19.

12. Daver N, Schlenk RF, Russell NH, Levis MJ. Targeting FLT3 mutations in AML: review of current knowledge and evidence. Leukemia 2019;33(2):299; doi: 10.1038/S41375-018-0357-9.
13. Döhner H, Weisdorf DJ, Bloomfield CD. Acute Myeloid Leukemia. N Engl J Med. 2015 Sep 17;373(12):1136-52. doi: 10.1056/NEJMra1406184.
14. Dugan J, Jain N, Irons C, Sharma P, Sediqe S, Hejal R. Differentiation syndrome after Gilteritinib: a tricky mimicker of sepsis. Chest 2021;160(4):A877; doi: 10.1016/j.chest.2021.07.820.
15. Essmann U, Perera L, Berkowitz ML, Darden T, Lee H, Pedersen LG. A smooth particle mesh Ewald method. J Chem Phys 1995;103(19):8577–8593; doi: 10.1063/1.470117.
16. Genheden S, Ryde U. The MM/PBSA and MM/GBSA methods to estimate ligand-binding affinities. Expert Opin Drug Discov 2015;10(5):449–461; doi: 10.1517/17460441.2015.1032936.
17. Gillessen A, Schmidt HHJ. Silymarin as Supportive Treatment in Liver Diseases: A Narrative Review. Adv Ther 2020;37(4):1279–1301; doi: 10.1007/S12325-020-01251-Y/FIGURES/1.
18. Guex N, Peitsch MC, Schwede T. Automated comparative protein structure modeling with SWISS-MODEL and Swiss-PdbViewer: A historical perspective. Electrophoresis 2009;30(SUPPL. 1):S162–S173.
19. Harrach MF, Drossel B. Structure and dynamics of TIP3P, TIP4P, and TIP5P water near smooth and atomistic walls of different hydroaffinity. Journal of Chemical Physics 2014;140(17); doi: 10.1063/1.4872239/317226.
20. Hollingsworth SA, Dror RO. Molecular Dynamics Simulation for All. Neuron 2018;99(6):1129–1143; doi: 10.1016/j.neuron.2018.08.011.
21. Hong L, Lei J. Scaling Law for Radius of Gyration and Its Dependence on Hydrophobicity. 2008. doi:10.1002/polb.21634
22. Islam MR, Islam Sovon MS, Amena U, Rahman M, Hosen ME, Kumer A, Bourhia M, Bin Jardan YA, Ibenmoussa S, Wondmie GF. Ligand-based drug design against Herpes Simplex Virus-1 capsid protein by modification of limonene through in silico approaches. Sci Rep. 2024;14(1):9828. doi: 10.1038/s41598-024-59577-4.
23. Ja'afaru SC, Uzairu A, Bayil I, Sallau MS, Ndukwe GI, Ibrahim MT, Moin AT, Mollah AKMM, Absar N. Unveiling potent inhibitors for schistosomiasis through ligand-based drug design, molecular docking, molecular dynamics simulations and pharmacokinetics predictions. PLoS One 2024;19(6):e0302390; doi: 10.1371/JOURNAL.PONE.0302390.
24. Jiang T, Li Y, Zhang N, Gan L, Su H, Xiang G, Wu Y, Liu Y. Unveiling unexpected adverse events: post-marketing safety surveillance of gilteritinib and midostaurin from the FDA Adverse Event Reporting database. Ther Adv Drug Saf 2025;16:20420986241308090; doi: 10.1177/20420986241308089.
25. Kalkan A, Pennig L, Pfister R, Cornely OA, Stemler J. Midostaurin-associated perimyocarditis: a case report of severe cardiotoxicity of novel targeted treatments for acute myeloid leukaemia and review of the literature. Eur Heart J Case Rep 2025;9(3); doi: 10.1093/EHJCR/YTAF044.
26. Kawase T, Nakazawa T, Eguchi T, Tsuzuki H, Ueno Y, Amano Y, Suzuki T, Mori M, Yoshida T. Effect of Fms-like tyrosine kinase 3 (FLT3) ligand (FL) on antitumor activity of gilteritinib, a FLT3 inhibitor, in mice xenografted with FL-overexpressing cells. Oncotarget 2019;10(58):6111–6123; doi: 10.18632/ONCOTARGET.27222.
27. Kim S, Chen J, Cheng T, Gindulyte A, He J, He S, Li Q, Shoemaker BA, Thiessen PA, Yu B, Zaslavsky L, Zhang J, Bolton EE. PubChem 2023 update. Nucleic Acids Res 2023;51(D1):D1373–D1380; doi: 10.1093/NAR/GKAC956.
28. Kiyoi H, Kawashima N, Ishikawa Y. FLT3 mutations in acute myeloid leukemia: Therapeutic paradigm beyond inhibitor development. Cancer Sci 2019;111(2):312; doi: 10.1111/CAS.14274.
29. Krieger E, Vriend G. New ways to boost molecular dynamics simulations. J Comput Chem 2015;36(13):996–1007.
30. Lagorce D, Douguet D, Miteva MA, Villoutreix BO. Computational analysis of calculated physicochemical and ADMET properties of protein-protein interaction inhibitors. Sci Rep. 2017;7:46277. doi: 10.1038/srep46277.
31. Lionta E, Spyrou G, Vassilatis DK, Cournia Z. Structure-Based Virtual Screening for Drug Discovery: Principles, Applications and Recent Advances. Curr Top Med Chem 2014;14(16):1923–1938; doi: 10.2174/1568026614666140929124445.
32. Lipinski CA, Lombardo F, Dominy BW, Feeney PJ. Experimental and Computational Approaches to Estimate Solubility and Permeability in Drug Discovery and Development Settings. Advanced Drug Delivery Reviews 1997;23(1–3):3-25.
33. Lipinski CA, Lombardo F, Dominy BW, Feeney PJ. Experimental and computational approaches to estimate solubility and permeability in drug discovery and development settings. Adv Drug Deliv Rev. 2001;46(1-3):3-26. doi: 10.1016/s0169-409x(00)00129-0.
34. Mecklenbrauck R, Heuser M. Resistance to targeted therapies in acute myeloid leukemia. Clin Exp Metastasis 2022;40(1):33; doi: 10.1007/S10585-022-10189-0.
35. Mirza Z, Al-Saedi DA, Alganmi N, Karim S. Landscape of FLT3 Variations Associated with Structural and Functional

Impact on Acute Myeloid Leukemia: A Computational Study. Int J Mol Sci 2024;25(6):3419; doi: 10.3390/IJMS25063419/S1.

36. Newcomer ME, Lewis BA, Quiocho FA. The radius of gyration of L-arabinose-binding protein decreases upon binding of ligand. Journal of Biological Chemistry 1981;256(24):13218–13222; doi: 10.1016/S0021-9258(18)43030-X.
37. O'Boyle NM, Banck M, James CA, Morley C, Vandermeersch T, Hutchison GR. Open Babel: An Open chemical toolbox. J Cheminform 2011;3(10):1–14; doi: 10.1186/1758-2946-3-33/FIGURES/1.
38. PDQ Adult Treatment Editorial Board. Adult Acute Myeloid Leukemia Treatment (PDQ®): Patient Version. PDQ Cancer Information Summaries 2002.
39. Perl AE, Martinelli G, Cortes JE, Neubauer A, Berman E, Paolini S, Montesinos P, Baer MR, Larson RA, Ustun C, Fabbiano F, Erba HP, Di Stasi A, Stuart R, Olin R, Kasner M, Ciceri F, Chou WC, Podoltsev N, Recher C, Yokoyama H, Hosono N, Yoon SS, Lee JH, Pardee T, Fathi AT, Liu C, Hasabou N, Liu X, Bahceci E, Levis MJ. Gilteritinib or Chemotherapy for Relapsed or Refractory FLT3-Mutated AML. N Engl J Med. 2019;381(18):1728-1740. doi: 10.1056/NEJMoa1902688. Erratum in: N Engl J Med. 2022;386(19):1868. doi: 10.1056/NEJMx220003.
40. Pires DEV, Blundell TL, Ascher DB. pkCSM: Predicting small-molecule pharmacokinetic and toxicity properties using graph-based signatures. J Med Chem 2015;58(9):4066–4072.
41. Razzaghi-Asl N, Mirzayi S, Mahnam K, Sepehri S. Identification of COX-2 inhibitors via structure-based virtual screening and molecular dynamics simulation. J Mol Graph Model 2018;83:138–152; doi: 10.1016/J.JMGM.2018.05.010.
42. Septembre-Malaterre A, Lalarizo Rakoto M, Marodon C, Bedoui Y, Nakab J, Simon E, Hoarau L, Savriama S, Strasberg D, Guiraud P, Selambarom J, Gasque P. Artemisia annua, a Traditional Plant Brought to Light. International Journal of Molecular Sciences 2020, Vol 21, Page 4986 2020;21(14):4986; doi: 10.3390/IJMS21144986.
43. Song X, Bao L, Feng C, Huang Q, Zhang F, Gao X, Han R. Accurate Prediction of Protein Structural Flexibility by Deep Learning Integrating Intricate Atomic Structures and Cryo-EM Density Information. Nat Commun. 2024;15(1):5538. doi: 10.1038/s41467-024-49858-x.
44. Stone RM, Mandrekar SJ, Sanford BL, Laumann K, Geyer S, Bloomfield CD, Thiede C, Prior TW, Döhner K, Marcucci G, Lo-Coco F, Klisovic RB, Wei A, Sierra J, Sanz MA, Brandwein JM, de Witte T, Niederwieser D, Appelbaum FR, Medeiros BC, Tallman MS, Krauter J, Schlenk RF, Ganser A, Serve H, Ehninger G, Amadori S, Larson RA, Döhner H. Midostaurin plus Chemotherapy for Acute Myeloid Leukemia with a FLT3 Mutation. N Engl J Med. 2017 Aug 3;377(5):454-464. doi: 10.1056/NEJMoa1614359.
45. Stumpfe D, Geppert H, Bajorath J. In Silico Screening. Lead Generation Approaches in Drug Discovery 2010;73–103; doi: 10.1002/9780470584170.ch3.
46. Tahamid Tusar MT, Hossen Z, Gazi HR, Haq N, Jubayer AA, Islam MM, Lisa AK, Sikdar B, Haque ME. High-throughput screening of natural antiviral drug candidates against white spot syndrome virus targeting VP28 in Penaeus monodon: Computational drug design approaches. J Genet Eng Biotechnol. 2025 Mar;23(1):100455. doi: 10.1016/j.jgeb.2024.100455.
47. Vivek-Ananth RP, Mohanraj K, Sahoo AK, Samal A. IMPPAT 2.0: An Enhanced and Expanded Phytochemical Atlas of Indian Medicinal Plants. ACS Omega 2023;8(9):8827–8845; doi: 10.1021/ACSOMEGA.3C00156.
48. Wang J, Wolf RM, Caldwell JW, Kollman PA, Case DA. Development and testing of a general Amber force field. J Comput Chem 2004;25(9):1157–1174.
49. Wang Y, Xing J, Xu Y, Zhou N, Peng J, Xiong Z, Liu X, Luo X, Luo C, Chen K, Zheng M, Jiang H. In silico ADME/T modelling for rational drug design. Q Rev Biophys 2015;48(4):488–515; doi: 10.1017/S0033583515000190.
50. Whayne TF. Clinical Use of Digitalis: A State of the Art Review. American Journal of Cardiovascular Drugs 2018; 18(6):427–440; doi: 10.1007/S40256-018-0292-1.